Çukurova Üniversitesi Mühendislik Mimarlık Fakültesi Dergisi, 27(1), ss. 39-51, Haziran 2012
Çukurova University Journal of the Faculty of Engineering and Architecture, 27(1), pp. 39-51, June 2012

Investigation of the Effects of Different Numerical Methods on the Solution of the Orifice Flow

Tural TUNAY[*1]
[1]*Çukurova University, Engineering & Architecture Faculty, Mechanical Engineering Department, Adana/Türkiye*

Abstract

Aim of the present study is to investigate the effects of different numerical methods on the solution of laminar flow characteristics through an orifice plate inserted in a pipe. Ratio of the orifice diameter to the pipe diameter, β=0.6 and dimensionless orifice plate thickness, L*=1/12, were kept constant throughout the study. The fluid flow was assumed to be two dimensional, axisymmetric, viscous, incompressible, steady and fully developed. Governing equations of the flow were solved with the aid of computer programs written in FORTRAN computer language by using two finite difference methods. These finite difference methods were alternating direction implicit method and upwind method. Additionally, finite volume method with the aid of Fluent package program was also employed to solve the flow for the purpose of comparison. Numerically obtained orifice discharge coefficient results were compared with experimental results obtained from literature. The best conformity with previous experimental results was obtained by using alternating direction implicit method. Vorticity contours, streamline and orifice discharge coefficient of the flow were presented in figures and discussed in details.

Key words: Numerical methods, discharge coefficient, laminar flow, orifice meter.

Çeşitli Sayısal Yöntemlerin Orifis Etrafındaki Akışın Sayısal Çözümüne Etkisinin İncelenmesi

Özet

Bu çalışmanın amacı boru içerisine yerleştirilmiş orifis metre etrafındaki laminar akış yapısının çözümüne farklı sayısal yöntemlerin etkisinin araştırılmasıdır. Orifis çapının boru çapına oranı β=0.6 ve boyutsuz orifis kalınlığı, L*=1/12 çalışma boyunca sabit tutulmuştur. Akış iki boyutlu, eksenel simetrik, viskoz, sıkıştırılamaz, daimi ve tam gelişmiş kabul edilmiştir. Akışı tanımlayan denklemler, FORTRAN programlama dili ile yazılmış bilgisayar programları kullanılarak, iki farklı sonlu farklar yöntemiyle çözülmüştür. Bu sonlu farklar yöntemleri, İmplisit Değişen Yönler yöntemi ve Upwind yöntemidir. Ayrıca elde edilen sayısal sonuçların karşılaştırılması amacıyla akış yapısı Fluent paket programı kullanılarak sonlu hacimler yöntemiyle de çözülmüştür. Sayısal yöntemlerle elde edilmiş olan debi çıkış katsayısı değerlerinin literatürden elde edilmiş olan deneysel değerler ile karşılaştırması yapılmıştır. Literatürden elde edilmiş deneysel sonuçlar ile en uyumlu sonucu implisit değişen yönler yöntemi vermiştir. Akışı tarif eden girdap eş değer eğrileri, akım çizgileri ve orifis debi çıkış katsayısı değerleri şekillerle gösterilerek detaylı bir şekilde izah edilmiştir.

Anahtar Kelimeler: Sayısal yöntemler, debi çıkış katsayısı, laminar akış, orifis metre.

[*] Yazışmaların yapılacağı yazar: Tural Tunay, Çukurova Üniversitesi, Müh. Mim. Fak., Makine Mühendisliği Bölümü, Adana. ttunay@cu.edu.tr

1. Introduction

There are various ways of measuring the flow rate of fluid flowing in a pipe. The most commonly used device for metering fluid flows is the orifice meter, which is a geometrically simple device. Working principle of the orifice meter is based on the measurement of the pressure difference created when forcing the fluid flow through them. The most important point in the design of orifice meter is the knowledge of discharge coefficient belonging to the orifice meter. Earlier experimental work of Johansen [1] has been on the flow discharge coefficient of water through a sharp-edged circular orifice for Re_o values in the range $0<Re_o\leq 5.7x10^4$ with the orifice/pipe diameter ratio, β varying from 0.2 to 0.8 for a constant orifice thickness/diameter ratio L^*. Here, Re_o is based on the orifice diameter.

The discharge coefficient, C_d for orifice meters is normally obtained by using empirical equations. These are based on the experimental data that are derived under a controlled laboratory conditions with having fully developed flow upstream of the orifice meter. In many field installations, however, it is not possible or practical to operate under conditions similar to those found in the laboratory applications. Departure from these conditions will change the characteristics of the flow field, and thereby alter the discharge coefficients. To improve experimental performance, computational fluid dynamics (CFD) models have been used to study and provide initial background for experimental studies [2]. Mills [3] have solved steady, axisymmetric, viscous, incompressible fluid flow around orifice plate inserted in the pipe numerically for $0 \leq Re_o \leq 50$ with β=0.5 whereby his predictions have agreed well with the experimental results of Johansen [1]. A solution technique through the rearrangement of the governing equations of the flow into a vorticity transport equation has been presented by Coder and Buckley [4]. Davis and Mattingly [5] have used the two-equation turbulence model developed for high Reynolds number flow through the orifice plates. Their turbulence model employed the eddy viscosity concept for the Reynolds stresses. In their study, the orifice plates were infinitely thin with orifice/pipe diameter ratios changing from β=0.4 to 0.7, Reynolds number range was $10^4\leq Re\leq 10^6$ and flow fields were modeled as axisymmetric. They have demonstrated that k-ε turbulence model can provide a reasonable accurate description of the important features of turbulent, incompressible flow through the axisymmetric, thin-plate orifice meter. Alvi et al. [6] have accomplished considerable experimental works on the flow characteristics around the sharp-edged orifices, quadrant-edged orifices and nozzles for $20\leq Re\leq 10^4$with varying β and constant L^* values. Numerical solution of the flow through the pipe orifice has also been studied by Nigro et al [7] and Nallasamy [8]. Cho and Goldstein [9] have presented a revised form of the low-Reynolds-number k-ε turbulence model that describes recirculating (separated and reattached) flows. Their revised model was well suited for low to moderate Reynolds numbers.

Çekici [10] has calculated stream function contours around the orifice plate by solving two-dimensional Navier Stokes equations in cartesian coordinates for Reynolds numbers in the range of $0\leq Re\leq 350$. Jones and Bajura [11] have executed the numerical solution of laminar pulsating flow through a 45-degree beveled pipe orifice by using stream function and vorticity transport equations for the range of $0.2\leq\beta\leq 0.5$ and $0<Re_o\leq 64$. Ma and Ruth [12] have developed vorticity circulation method for contracting flow to calculate vorticity values around the re-entrant sharp corner.

Extensive experimental and numerical investigations of steady, laminar, incompressible and axisymmetric flow around the square-edged orifice inserted in the pipe have been carried out by Şahin and Ceyhan [13]. Further numerical investigations of the flow characteristics around the similar flow geometry by employing finite element method have conducted by Şahin and Akıllı [14] for the range of $0\leq Re_o\leq 2000$, $1/16\leq L^*\leq 1$ and $0.2\leq\beta\leq 0.9$. Erdal and Andersson [2] have studied modeling of the flow through the orifice plates. They have started their studies with a full pipe simulation in order to investigate various grid effects, coordinate arrangements, wall

boundary conditions, differencing schemes and turbulence models that can predict more accurate flow values through the orifice plate. Their calculations were carried out in two-dimensional axisymmetric flow. Gan and Riffat [15] have conducted a CFD study to understand the effect of plate thickness on the pressure loss characteristics of the square edged orifice located in a square duct for a range of Reynolds numbers. Ramamurthi and Nandakumar [16] conducted studies on the flow through small sharp-edged cylindrical orifices to determine characteristics of the flow in the separated, attached and cavitated flow regions.

Tunay [17] have conducted studies to investigate the characteristics of laminar and turbulent flow through the pipe orifice with various orifice thicknesses. Tunay et al. [18, 19] have also investigated effects of different boundary conditions on the numerical solutions of the laminar flow characteristics through the orifice plate inserted in the pipe with the aid of vorticity-transport equations.

Considerable research efforts in investigation of the orifice flow have been continued in recent years. These orifices typically have diameter ratios, β in the range of 0.2 to 0.75 and orifice thickness/diameter ratios, L^* less than 1 [20, 21, 22, 23, 24].

In the present study, effects of the different numerical methods on the solution of the orifice flow were investigated by using two finite difference schemes called upwind and alternating direction implicit methods and finite volume techniques via Fluent package program for fully-developed, incompressible, viscous, axisymetric, steady and laminar flow. A computer code was developed for the part of the present work in which finite difference methods were used. Here, orifice/pipe diameter ratio, β= 0.6 and dimensionless orifice plate thickness, L^*=1/12 were kept constant throughout the work.

2. Material and Methods

Navier-Stokes and continuity equations were used as fundamental equations and flow was assumed to be steady, viscous, fully developed, incompressible, laminar and axisymmetric. Equations governing this type of flow are expressed as follows.

Navier-Stokes equations:

$$\frac{\partial V_r}{\partial t} + V_r \frac{\partial V_r}{\partial r} + V_z \frac{\partial V_r}{\partial z} = -\frac{1}{\rho}\frac{\partial P}{\partial r} + \nu\left(\frac{\partial^2 V_r}{\partial r^2} + \frac{1}{r}\frac{\partial V_r}{\partial r} - \frac{V_r}{r^2} + \frac{\partial^2 V_r}{\partial z^2}\right) \quad (1.a)$$

$$\frac{\partial V_z}{\partial t} + V_r \frac{\partial V_z}{\partial r} + V_z \frac{\partial V_z}{\partial z} = -\frac{1}{\rho}\frac{\partial P}{\partial z} + \nu\left(\frac{\partial^2 V_z}{\partial r^2} + \frac{1}{r}\frac{\partial V_z}{\partial r} + \frac{\partial^2 V_z}{\partial z^2}\right) \quad (1.b)$$

Continuity equation:

$$\frac{\partial V_r}{\partial r} + \frac{V_r}{r} + \frac{\partial V_z}{\partial z} = 0 \quad (2)$$

where V_r and V_z are radial and axial component of velocity, P is pressure, ρ is density, t is time. The time derivative of velocity components was left in equations (1.a and 1.b) consciously, because of the fact that stability can be obtained more quickly with parabolic equations. This addition of term has no physical meaning. Following group of equations was used to obtain dimensionless form of the governing equations. Here "*" was used to denote dimensionless form of the flow parameters.

$$V_r^* = \frac{V_r}{\bar{V}},\ V_z^* = \frac{V_z}{\bar{V}},\ z^* = \frac{z}{R},\ r^* = \frac{r}{R},$$

$$Re = \frac{\rho \bar{V} D}{\mu},\ P^* = \frac{P}{\frac{1}{2}\rho(2\bar{V})^2},\ \psi^* = \frac{\psi}{\bar{V}R^2}, \quad (3)$$

$$\omega^* = \frac{\omega R}{\bar{V}},\ L^* = \frac{L}{d_o},\ t^* = \frac{t\bar{V}}{R}$$

where ω is vorticity, ψ is stream function, $\bar{V}$ is average flow velocity, L is thickness of the orifice

plate, R is radius of the pipe and d_o is radius of the orifice plate.

Vorticity transport equation (4) and stream function equation (5) can be written as follows by using governing equations (1 and 2) and the group of dimensionless parameters (3) shown above.

$$\frac{\partial^2\omega^*}{\partial r^{*2}}+\frac{\partial^2\omega^*}{\partial z^{*2}}=\frac{1}{r^*}\left(\frac{\omega^*}{r^*}-\frac{\partial\omega^*}{\partial r^*}\right)+\frac{Re}{2}\left(\frac{\partial\omega^*}{\partial t^*}+\frac{1}{r^*}\frac{\partial\psi^*}{\partial z^*}\frac{\partial\omega^*}{\partial r^*}-\frac{1}{r^*}\frac{\partial\psi^*}{\partial r^*}\frac{\partial\omega^*}{\partial z^*}-\frac{\omega^*}{r^{*2}}\frac{\partial\psi^*}{\partial z^*}\right) \tag{4}$$

$$\frac{\partial^2\psi^*}{\partial r^{*2}}+\frac{\partial^2\psi^*}{\partial z^{*2}}=r^*\omega^*+\frac{1}{r^*}\frac{\partial\psi^*}{\partial r^*} \tag{5}$$

For the calculation of discharge coefficient, static pressure distribution along the pipe was calculated. Pressure distributions can be determined by integrating dimensionless form of Navier-Stokes equations shown below with the aid of Simpson's 1/3 integration rule.

$$V_r^*=\frac{1}{r^*}\frac{\partial\psi^*}{\partial z^*} \tag{6}$$

$$V_z^*=-\frac{1}{r^*}\frac{\partial\psi^*}{\partial r^*} \tag{7}$$

$$2\frac{\partial P^*}{\partial r^*}=\frac{2}{Re}\left(\frac{\partial^2V_r^*}{\partial r^{*2}}+\frac{1}{r^*}\frac{\partial V_r^*}{\partial r^*}-\frac{V_r^*}{r^{*2}}+\frac{\partial^2V_r^*}{\partial z^{*2}}\right)-\left(V_r^*\frac{\partial V_r^*}{\partial r^*}+V_z^*\frac{\partial V_r^*}{\partial z^*}\right) \tag{8}$$

$$2\frac{\partial P^*}{\partial z^*}=\frac{2}{Re}\left(\frac{\partial^2V_z^*}{\partial r^{*2}}+\frac{1}{r^*}\frac{\partial V_z^*}{\partial r^*}+\frac{\partial^2V_z^*}{\partial z^{*2}}\right)-\left(V_r^*\frac{\partial V_z^*}{\partial r^*}+v_z^*\frac{\partial V_z^*}{\partial z^*}\right) \tag{9}$$

2.1. Flow Geometry

Because fully developed flow condition was assumed at the inlet of the pipe, an orifice plate which was placed 4D from the inlet and 23D from the exit of the pipe was used. The orifice plate employed had a concentric hole. Schematic of the square-edged orifice plate inserted in the circular pipe is shown in Figure 1. In this figure, cross sections 1 and 2 represent the locations of pressure taps used for the numerical calculation of the orifice discharge coefficient. The length between the location of the upstream tapping point and the inlet surface of the orifice was one diameter of the pipe, D. The length between the downstream pressure tapping and the inlet surface of the orifice was one half of the pipe diameter, D/2.

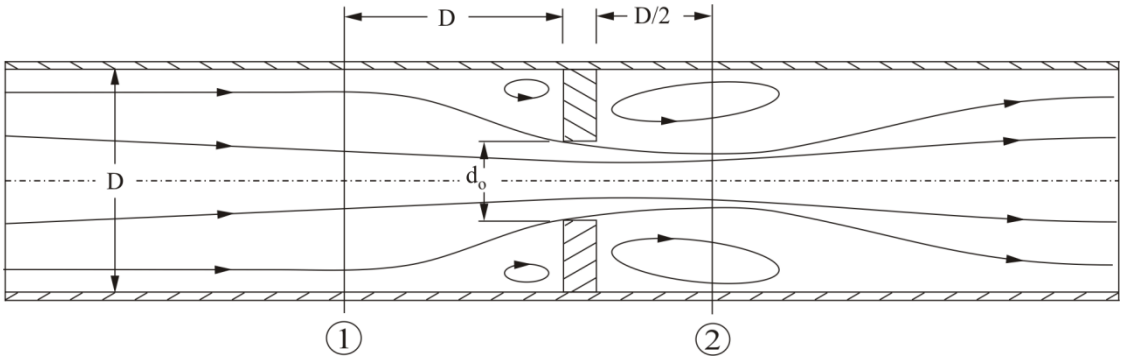

Figure 1. Square-edged orifice meter inserted in the circular pipe.

As known from previous studies [13, 19, 20] that the orifice discharge coefficient is a function of the orifice thickness/diameter ratio (L^*), orifice/pipe diameter ratio (β) and Reynolds number (Re). In practice, the accuracy of the measurement of the volume flow rate strongly depends on the accurate measurement of the pressure differential, which is caused by the orifice plate. The relationship between the pressure differential and the volume flow rate can be characterized by the discharge coefficient, C_d. The orifice discharge coefficient for steady flow has been defined by applying the continuity and Bernoulli equations to the flow geometry shown in Figure 1.

$$C_d = \frac{1}{2\sqrt{2}}\left(\frac{1}{\beta}\right)^2\left(1-\beta^4\right)^{1/2}\frac{1}{\sqrt{\Delta P^*}} \qquad (10)$$

Here ΔP^* is the dimensionless pressure difference between cross sections 1 and 2 shown in Figure 1.

2.2. Initial and Boundary Conditions

- The simulated pipe geometry and notation used for the boundary conditions are presented in Figure 2. A fully developed laminar flow was assumed to exist at the inlet cross section of the pipe (AB). Therefore, the radial velocity component, V_r is equal to zero and the equation for the parabolic velocity profile at the inlet boundary is determined as follow.

$$V_z = V_{z,max}\left(1-\left(\frac{r}{R}\right)^2\right) \qquad (11)$$

- Since the flow was assumed to be axially symmetric, only one half of the flow domain was considered throughout the calculations and the term $\frac{\partial V_z}{\partial r}$ was taken as zero at the central axis of the pipe. Radial velocity component should be zero along the centreline of the pipe (AH). At the pipe walls, no slip boundary condition was used. Therefore velocity components V_r and V_z were equal to zero at the pipe walls. At the outlet (GH), the diffusion fluxes for all flow variables in the flow direction were taken as zero.

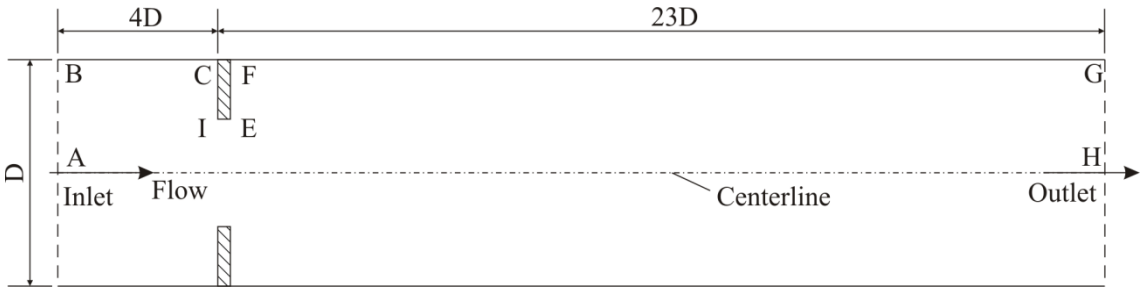

Figure 2. The simulated pipe geometry and notation for the boundary conditions (The dimensions are not scaled).

The following equation for the stream function can be written as the inlet boundary condition for laminar fully developed flow. The value of stream function through the centreline was constant. If above conditions are satisfied, the value of stream function on the pipe wall (through BC, CI, IE, EF and FG) should also be constant. On the boundaries BC, CI, IE, EF and FG, the value of stream function became $\psi^* = 0.5$. On the central axis, the value of stream function was equal to zero.

$$\psi^* = r^{*2}\left(1-\frac{r^{*2}}{2}\right) \qquad (12)$$

The resulting equation for the vorticity at the inlet was found by using equation (13). According to this equation, vorticitiy value at the centreline (AH) was zero.

$$\omega^{*}=4r^{*} \tag{13}$$

To calculate vorticity values at the pipe walls for axisymmetric flow conditions, we employed equations recommended by Lester [25]. He has considered vertical and horizontal walls separately for his calculations of the flow characteristics around the orifice. These equations can be given as follows.

For horizontal wall:

$$\omega_{i,j}^{*}=\frac{\frac{6}{H^{2}r_{i}^{*}}\left(\psi_{i\pm1,j}^{*}-\psi_{i,j}^{*}\right)-\frac{r_{i+1}^{*}}{r_{i}^{*}}\omega_{i\pm1,j}^{*}}{2+\frac{H}{r_{i}^{*}}-\frac{H^{2}}{4r_{i}^{*2}}} \tag{14}$$

For vertical wall:

$$\omega_{i,j}^{*}=\frac{3}{H^{2}r_{i}^{*}}\left(\psi_{i,j\pm1}^{*}-\psi_{i,j}^{*}\right)-\frac{1}{2}\omega_{i,j\pm1}^{*} \tag{15}$$

Furthermore, for the corner vorticity values, average of two vorticity values at the adjacent grids on the vertical and horizontal walls were used as presented in equation (16).

$$\omega_{c}^{*}=\frac{\omega_{a}^{*}+\omega_{b}^{*}}{2}=\frac{\psi_{ic,jc}^{*}-\psi_{ic-1,jc}^{*}}{r_{jc}^{*}H^{2}}+\frac{\psi_{ic,jc}^{*}-\psi_{ic,jc-1}^{*}}{r_{jc}^{*}H^{2}} \tag{16}$$

2.3. Discretization of Governing Equations

For the numerical investigations, governing equations of the flow were solved with the aid of computer programs written in FORTRAN computer language by two using finite difference methods. These finite difference methods were alternating direction implicit method and upwind method. Additionally, finite volume method with the aid of Fluent package program was also employed to solve the flow domain for the purpose of comparison.

2.3.1. The Upwind Differencing Method

This method has often been used in the literature under various names and with different rationales [26]. Ordinary central difference methods do not always follow the proper flow of information throughout the flow field. Upwind schemes are designed numerically to simulate more properly the direction of the propagation of information in a flow field [27]. In addition to that, using upwind differencing gives an unconditionally stable computation scheme for the vorticity equation. Vorticity transport equation (4) was discretized by using upwind differencing method as follow. Here, (i) and (j) notations were used for terms in axial and radial directions, respectively.

$$\begin{aligned}&\frac{2}{Re}\left(\frac{\omega_{i,j-1}^{*n+1}-2\omega_{i,j}^{*n+1}+\omega_{i,j+1}^{*n+1}}{H^{2}}+\frac{\omega_{i-1,j}^{*n}-2\omega_{i,j}^{*n+1}+\omega_{i+1,j}^{*n}}{H^{2}}\right)=\frac{2}{Re}\left(\frac{\omega_{i,j}^{*n+1}}{r_{j}^{*2}}-\frac{1}{r_{j}^{*}}\frac{\omega_{i,j+1}^{*n+1}-\omega_{i,j-1}^{*n+1}}{2H}\right)\\&+\frac{\omega_{i,j}^{*n+1}-\omega_{i,j}^{*n}}{\Delta t^{*}}+\frac{1}{2H}\left(-\omega_{i,j-1}^{*n+1}\left(v_{r_{i,j}}^{*n}+\left|v_{ri,j}^{*n}\right|\right)+\omega_{i,j+1}^{*n+1}\left(v_{r_{i,j}}^{*n}-\left|v_{r_{i,j}}^{*n}\right|\right)+2\omega_{i,j}^{*n+1}\left|v_{r_{i,j}}^{*n}\right|\right)\\&+\frac{1}{2H}\left(-\omega_{i-1,j}^{*n}\left(v_{z_{i,j}}^{*n}+\left|v_{z_{i,j}}^{*n}\right|\right)+\omega_{i+1,j}^{n}\left(v_{z_{i,j}}^{*n}-\left|v_{z_{i,j}}^{*n}\right|\right)+2\omega_{i,j}^{*n+1}\left|v_{z_{i,j}}^{*n}\right|\right)-\frac{\omega_{i,j}^{*n+1}v_{r_{i,j}}^{*n}}{r_{j}^{*}}\end{aligned} \tag{17}$$

where H is distance between two grids in both axial and vertical directions. Equation (17) can easily be solved by reducing to three diagonal matrix forms.

2.3.2. Alternating Direction Implicit Method

This method makes use of a splitting of the time step to obtain a multi-dimensional implicit method, which requires only the inversion of a tridiagonal matrix. In this method, values of $\omega^{*}(t+\Delta t)$ were obtained in some fashion from the known values of $\omega^{*}(t)$. The solution of $\omega^{*}(t+\Delta t)$ was achieved in a two step process, where intermediate values of ω^{*} were found at an intermediate time, $(t+\Delta t/2)$. In the first step, over a time interval $\Delta t/2$, the spatial derivatives in equation (4) were replaced

with central differences, where only the z derivative was treated implicitly and the following equation was yielded.

$$\frac{Re}{2}\frac{\omega^{*n+1/2}_{i,j}-\omega^{*n}_{i,j}}{\Delta t^{*}/2}+\frac{Re}{2}V_r^{*n}\frac{\omega^{*n}_{i,j+1}-\omega^{*n}_{i,j-1}}{2H}+\frac{Re}{2}V_z^{*n}\frac{\omega^{*n+1/2}_{i+1,j}-\omega^{*n+1/2}_{i-1,j}}{2H}-\frac{Re}{2}\frac{V_r^{*n}}{r^{*}}\omega^{*n+1/2}_{i,j}$$
$$=\frac{\omega^{*n}_{i,j-1}-2\omega^{*n}_{i,j}+\omega^{*n}_{i,j+1}}{H^2}+\frac{\omega^{*n+1/2}_{i-1,j}-2\omega^{*n+1/2}_{i,j}+\omega^{*n+1/2}_{i+1,j}}{H^2}-\frac{\omega^{*n+1/2}_{i,j}}{r^{*2}}+\frac{1}{r^{*}}\frac{\omega^{*n}_{i,j+1}-\omega^{*n}_{i,j-1}}{2H} \quad (18)$$

The second step of the alternating direction implicit method takes the solutions of ω^{*} for time $t+\Delta t$, using the known values at time $t+\Delta t/2$. For this second step, the spatial derivatives in equation (4) were replaced with central differences, where the r derivative was treated implicitly. Hence, equation (4) can be obtained as follow.

$$\frac{Re}{2}\frac{\omega^{*n+1}_{i,j}-\omega^{*n+1/2}_{i,j}}{\Delta t^{*}/2}+\frac{Re}{2}V_r^{*n}\frac{\omega^{*n+1}_{i,j+1}-\omega^{*n+1}_{i,j-1}}{2H}+\frac{Re}{2}V_z^{*n}\frac{\omega^{*n+1/2}_{i+1,j}-\omega^{*n+1/2}_{i-1,j}}{2H}-\frac{Re}{2}\frac{V_r^{*n}}{r^{*}}\omega^{*n+1}_{i,j}$$
$$=\frac{\omega^{*n+1}_{i,j-1}-2\omega^{*n+1}_{i,j}+\omega^{*n+1}_{i,j+1}}{H^2}+\frac{\omega^{*n+1/2}_{i-1,j}-2\omega^{*n+1/2}_{i,j}+\omega^{*n+1/2}_{i+1,j}}{H^2}-\frac{\omega^{*n+1}_{i,j}}{r^{*2}}+\frac{1}{r^{*}}\frac{\omega^{*n+1}_{i,j+1}-\omega^{*n+1}_{i,j-1}}{2H} \quad (19)$$

Again, here, H is the distance between two grids in both axial and vertical directions. Equations (18) and (19) can be reduced to three diagonal matrix forms.

Stream function equation was solved with the aid of successive relaxation method as follow.

$$\psi^{*n+1}_{i,j}=0.25\left(\psi^{*}_{i+1,j}+\psi^{*}_{i-1,j}+\psi^{*}_{i,j-1}+\psi_{i,j+1}\right)-\frac{H}{8r^{*}_{j}}\left(\psi^{*}_{i,j+1}-\psi^{*}_{i,j-1}\right)+\frac{H^2r^{*}_{j}}{4}\omega^{*}_{i,j} \quad (20)$$

2.3.3. Finite Volume Method

Governing equations were also discretized using finite volume method with the aid of Fluent package program. The numerical method employed to linearize and solve the discretized governing equations was rely on the pressure-based segregated algorithm. In this algorithm the momentum and continuity equations are solved sequentially wherein the constraint of mass conservation of the velocity field is achieved by solving a pressure correction equation. The pressure equation is derived from the continuity and the momentum equations in such a way that the velocity field, corrected by the pressure, satisfies the continuity. The SIMPLEC (Semi-Implicit Method for Pressure-Linked Equations-Consistent) algorithm was used for introducing pressure into the continuity equation. In simulations, a co-located scheme was used, whereby pressure and velocity are both stored at cell centres. Standard pressure interpolation scheme was used to compute required face values of pressure from the cell values. In simulations, face values of scalars required for the convection terms in the discretized governing equation were interpolated from the discrete values of the scalar stored at the cell centers. This was accomplished by using QUICK scheme**.** A point implicit (Gauss-Seidel) linear equation solver was used in conjunction with an Algebraic Multigrid (AMG) method to solve the resultant scalar system of equations for the dependent variable in each cell.

3. Results and Discussions

In this work, investigation of the results of different numerical methods on the solution of the flow characteristics around the square-edged orifice plate inserted in the pipe was aimed. Flow was assumed to be viscous, incompressible, axisymmetric, steady and two-dimensional. Orifice/pipe diameter ratio, $\beta=0.6$ and dimensionless orifice plate thickness, $L^{*}=1/12$, were kept constant throughout the work. Equations governing the flow have been solved by using upwind and alternating direction implicit methods of finite difference method. To allow the

comparison of the numerical methods used, governing equations were also solved by using finite volume method. Numerical results obtained in the present work were also compared with corresponding experimental data taken from the open literature.

A grid independency study was performed to find a grid that was sufficiently fine to provide accurate solutions. In order to check the grid independency of the calculations, predictions of the discharge coefficient with various size of the mesh inserted in the flow field at Reynolds number of 400 were carried out. Comparison of the discharge coefficient for different grid sizes for all numerical methods employed in this study is given in Figure 3. In this figure, it is observed that beyond the grid size of 56x3024, change in the value of the orifice discharge coefficient is negligible. Therefore, 56x3024 was selected as the grid size of the present study and the flow field was divided into 55 intervals in the vertical direction and 3023 intervals in the horizontal direction for the investigation.

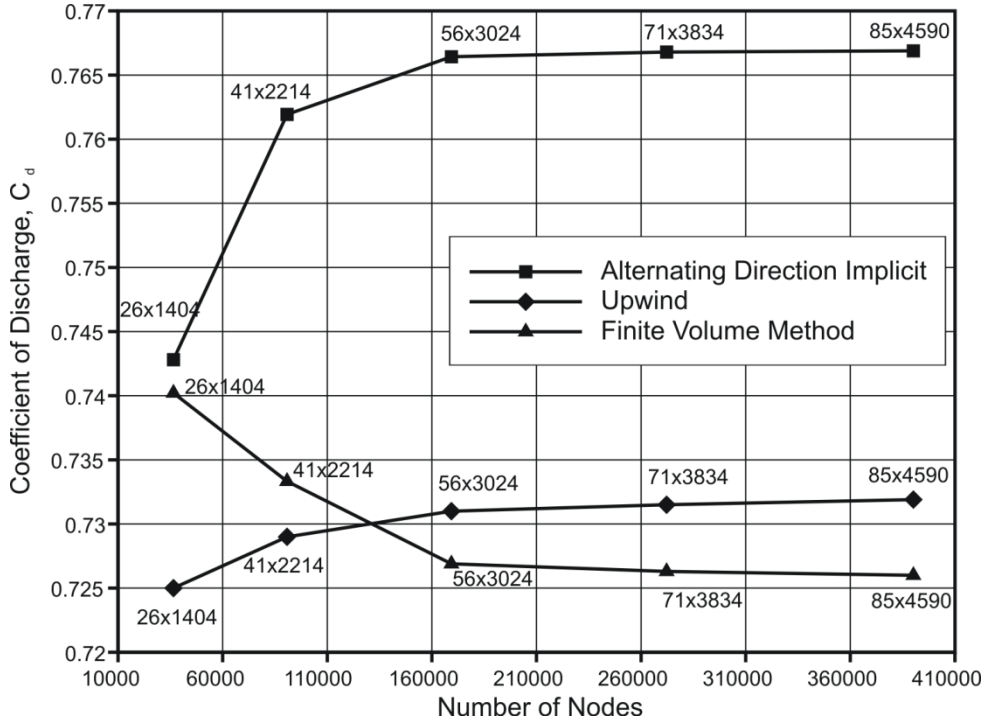

Figure 3. Variation of the orifice discharge coefficient with different mesh sizes at Reynolds number of 400

General information about the flow can be obtained from contours of vorticity and stream functions. Therefore, contours of stream function and vorticity obtained at each grid point in the flow field by using finite volume method, alternating direction implicit method and upwind method are presented for Reynolds numbers, Re=36, 400 and 625 in Figures 4-6. Due to the axial symmetry of the flow field, vorticity contours are shown in the upper part of the figures, and in the lower part of the figures streamlines are given.

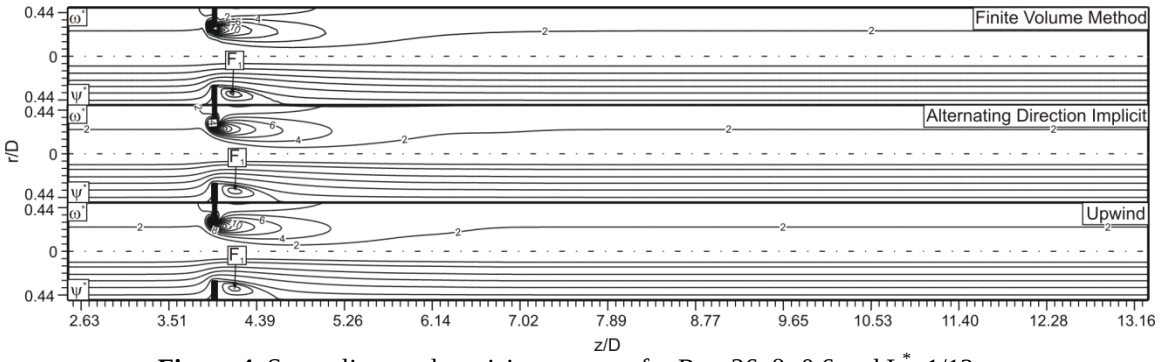

Figure 4. Streamlines and vorticity contours for Re_o=36, β=0.6 and L^*=1/12.

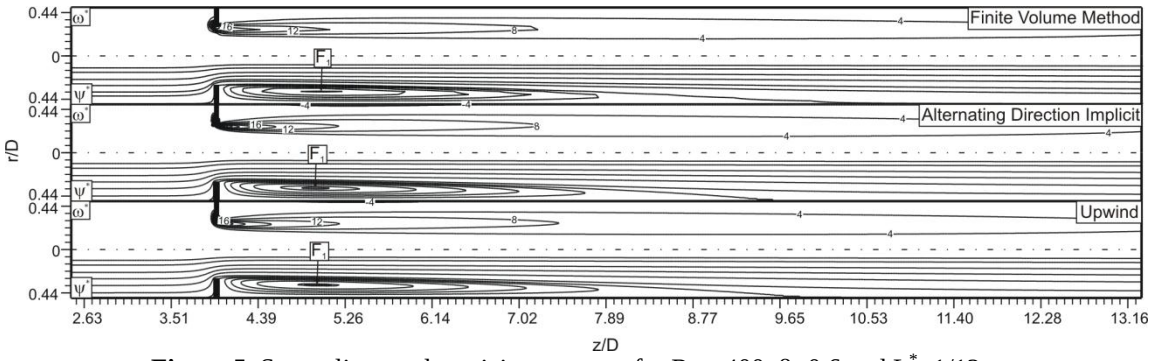

Figure 5. Streamlines and vorticity contours for Re_o=400, β=0.6 and L^*=1/12.

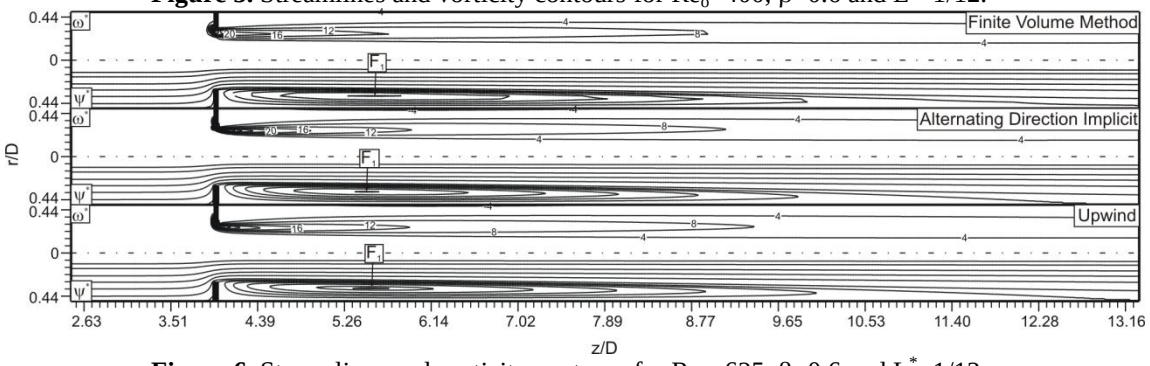

Figure 6. Streamlines and vorticity contours for Re_o=625, β=0.6 and L^*=1/12.

In above figures, it is observed that the maximum variations of the flow characteristics occur around the orifice plate for all numerical results obtained. As the flow enters into the region where the effect of the orifice plate exists, parallel structure of the flow begins to deteriorate. While flow moves further downstream, it begins to separate away at the inlet edge of the orifice and flow streamlines tend to converge to form a jet. This flow jet continue to contract as the flow moves downstream and develops a minimum cross sectional area at some distance downstream of the orifice plate called as vena contracta. The size of the separated flow region after the orifice plate increases in radial direction until the vena contracta. After the vena contracta, the flow jet expands gradually in axial direction and reattaches to the pipe wall at a point further downstream. The length of the separated flow region is proportional to Reynolds number as shown in Figures 4-6.

Additionally, occurrence of the separation at the rare side of the orifice plate causes further increase in pressure loss. As is the case in stream function, as the Reynolds number increases, the size and magnitude of vorticity contours increase along the flow direction. In Table 1, comparisons of the location of the focus, F_1 calculated by using different numerical methods are given. It is interesting that as the Reynolds number increases, location of the focus, F_1 does not change considerably in the vertical direction. In addition to that in the stream-wise direction, location of the focus, F_1 goes further downstream as the Reynolds number increase. Location of the focus, F_1 results of all numerical methods considered here are consistent with each other.

Table 1. Comparisons of the location of the focus, F_1.

	Re_o=36		Re_o=400		Re_o=625	
	z/D	r/D	z/D	r/D	z/D	r/D
Upwind	0.170	0.383	1.023	0.362	1.576	0.366
Alternating Direction Implicit	0.173	0.378	0.991	0.365	1.526	0.365
Finite Volume Method	0.156	0.382	1.058	0.368	1.611	0.371

In Table 2, comparisons of the length of the separated flow region after the orifice plate calculated by using different numerical methods are given. Here it is clearly seen that as the Reynolds number increase, length of the separated flow region increase considerably. Finite volume method calculated the length of the separated flow region longer than the other methods. Results of upwind method and alternating direction method show similar results with each other.

Table 2. Variation of the length of the separated flow region.

	Re_o=36	Re_o=400	Re_o=625
	z/D	z/D	z/D
Upwind	0.636	6.007	9.419
Alternating Direction Implicit	0.640	5.737	8.968
Finite Volume Method	0.692	6.683	9.799

Variations of orifice discharge coefficient with Reynolds number obtained by using different numerical methods are provided in Figure 7 for the constant value of t^*=1/12 and β=0.6. Present results are compared with the experimental results of Johansen [1] and Alvi et al. [6]. Due to the fact that all aspects of the orifice geometry can have a considerable influence on the pressure distributions and flow characteristics, a rapid variation occurs in the values of discharge coefficients at low Reynolds numbers. We know from the previous studies conducted by Şahin and Ceyhan [13] and Tunay et al. [19, 20], the values of discharge coefficient calculated with respect to Reynolds number, $Re_o \leq 105$ changes rapidly. Beyond this level of Reynolds number, the value of discharge coefficient varies approximately in between C_d= 0.72~0.77 for β=0.6. The results of the discharge coefficients of all numerical methods employed in the present study also exhibit a large gradient of change at Reynolds numbers in the range $1 \leq Re_o \leq 100$.

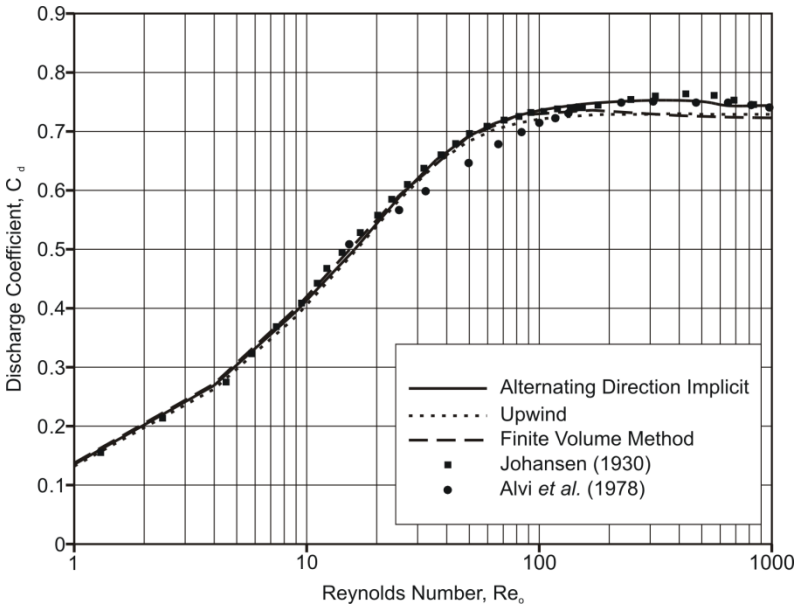

Figure 7. Comparison of the variation of the orifice discharge coefficient with Reynolds number for β=0.6.

Results obtained by using upwind method and finite volume method have a good agreement with previous experimental results for Reynolds numbers range of $Re_o \leq 200$. However as the Reynolds number increases, their conformity with experimental results deteriorates. The maximum deviation between the present and previous experimental results is approximately 3.9% above $Re_o \geq 200$. It is thought that the similarity observed between the results of upwind method and finite volume method is due to the fact that in finite volume method we employ QUICK method, which is derivative of upwind method for the discretization of the momentum equations. For Reynolds number in the range of $Re_o \leq 80$, all dataset indicate a good conformity with each other but as the Reynolds number increases this conformity deteriorates. The results of the alternating direction implicit method have a good agreement with experimental results at all Reynolds numbers especially with results of Johansen (1930). On the other hand, this conformity deteriorates for small range of Reynolds numbers, $Re_o \leq 20$.

4. Conclusions

In this study, effects of different numerical methods on the solution of the orifice flow were investigated by using finite volume method and two finite difference schemes called upwind and alternating direction implicit methods for fully-developed, incompressible, viscous, axisymetric, steady and laminar flow. Calculated results of orifice discharge coefficients were compared with previous experimental results. The best conformity with previous experimental results was obtained by using alternating direction implicit method. Locations of the focus, F1 calculated by numerical methods show more or less similar results. In addition to that finite volume method calculated the length of the separated flow region longer than the other two methods considered.

5. References

1. Johansen, F. C., "Flow Through Pipe Orifices at Low Reynolds Numbers", Proc R Soc, 126 (Series A), 231, 1930.

2. Erdal, A. and Andersson, H. I., "Numerical Aspects of Flow Computation Through

Orifices", Flow Measurement and Instrumentation, Vol. 8, No. 1, pp. 27-37, 1997.

3. Mills, R. D., "Numerical Solutions of Viscous Flow Through a Pipe Orifice at Low Reynolds Numbers", Mechanical Engineering Science, 10(2), 133-140, 1968.

4. Coder, D. A. and Buckley, F. T., "Implicit Solutions of the Unsteady Navier-Stokes Equation For Laminar Flow Through an Orifice Within a Pipe", Computers and Fluids, Vol.2, pp. 295-314, 1974.

5. Davis, R.W. and Mattingly, G.E., "Numerical Modelling of Turbulent Flow Through Thin Orifice Plates", Proceedings of the Semp. on Flow in Open Channels and Closed Conduits Held at NBS, 23-25 February 1977.

6. Alvi, S. H., Sridharan, K., and Lakshmana Rao, N. S., "Loss Characteristics of Orifices and Nozzles", Journals of Fluids Engineering, 100, 299-307, 1978.

7. Nigro, F. E. B., Strong, A. B. and Alpay, S. A., "A Numerical Study of the Laminar Viscous Incompressible Flow Through a Pipe Orifice", Journal of Fluids Engineering, Vol.100, pp. 467-472, 1978.

8. Nallasamy, M., "Numerical Solution of the Separating Flow Due to an Obstruction", Computers and Fluids, Vol. 14, No. 1, pp. 59-68, 1986.

9. Cho and Goldstein, "An improved low-Reynolds-number κ-ε turbulence model for recirculating flows", International Journal of Heat and Mass Transfer, 37, 10, 1495-1508, 1994.

10. Çekici, V., "Orifislerde Düşük Reynolds Sayılarındaki Akış Karakteristiklerinin İncelenmesi", MSc. Thesis, Çukurova University Institute of Natural and Applied Sciences, 1991.

11. Jones, E. H. and Bajura, R. A., "A Numerical Analysis of Pulsating Laminar Flow Through a Pipe Orifice", Journal of Fluids Engineering, Vol. 113, no. 2, pp. 199-205, 1991.

12. Ma, H. and Ruth, D.W., "A New Scheme for Vorticity Computations Near a Sharp Corner", Computers and Fluids, Vol.23, No.1, pp 23-38, 1994.

13. Sahin, B. and Ceyhan, H., "A Numerical and Experimental Analysis of Laminar Flow Through Square Edged Orifice with a Variable Thickness", Transactions of the Institute of Measurement and Control, Vol.18, No.4, pp.166-173, 1996.

14. Sahin, B., and Akıllı, H., "Finite Element Solution of Laminar Flow Through Square-Edged Orifice with a Variable Thickness", International Journal of Computational Fluid Dynamics, Vol.9, pp.85-88, 1997.

15. Gan, G. and Riffat, S. B., "Pressure Loss Characteristics of Orifice and Perforated Plates", Experimental Thermal and Fluid Science, Vol.14, pp. 160-165, 1997.

16. Ramamurthi, K. and Nandakumar, K., "Characteristics of flow through small sharp-edged cylindrical orifices", Flow Measurement and Instrumentation, Vol. 10, pp. 133–143, 1999.

17. Tunay, T., "Investigation of Laminar and Turbulent Flow Characteristics through Orifice with Variable Thicknesses", MSc. Thesis, Çukurova University Institute of Natural and Applied Sciences, 2002.

18. Tunay, T., Kahraman, A. and Şahin, B., 2002. "Orifis Yerleştirilmiş Borudaki Akışın Sayısal Çözümüne Sınır Şartlarının Etkisi", GAP 4. Mühendislik Kongresi, Şanlıurfa.

19. Tunay, T., Kahraman, A. and Şahin, B., 2011. "Effects of the Boundary Conditions on the Numerical Solution of the Orifice Flow", Ç.Ü. Müh. Mim. Fak. Dergisi, accepted for publication.

20. Tunay, T., Sahin, B. and Akıllı, H., "Investigation of Laminar and Turbulent flow through an orifice plate inserted in a pipe", Transactions of the Canadian Society for Mechanical Engineering, 28 (2B), 403-414, 2004.

21. Bohra, L. K., "Flow and Pressure Drop of Highly Viscous fluids in Small Aperture Orifices". MSc. Thesis, Georgia Institute of Technology**,** 2004.

22. Mishra, C. and Peles, Y., "Incompressible and Compressible Flows through Rectangular Microorifices Entrenched in Silicon Microchannels", Journal of Microelectromechanical Systems, Vol. 14, No. 5, 1000-1012, 2005.

23. Maldonado, J. J. C. and Benavides, D. N. M., "Computational Fluid Dynamics (CFD) and Its Application in Fluid Measurement Systems", International Symposium on Fluid Flow Measurement, 16-18 May 2006.

24. Chen, J., Wang, B., Wu, B. and Chu, Q., "CFD Simulation of Flow Field in Standard Orifice Plate Flow Meter", *Journal of Experiments in Fluid Mechanics*, Vol. 22, No. 2, pp. 51-55, 2008.

25. Lester, W. G. S., "The Flow Past a Pitot Tube at Low Reynolds Numbers", Report and Memoranda Aeronautical Research Committee, No 3240, 1-23, 1960.

26. Roache, P. J., "Computational Fluid Dynamics", Hermosa Publishers, U.S.A., 1972.

27. Anderson, J., "Computational Fluid Dynamics", McGraw-Hill Press, U.S.A., 1995.